

CERN-PH-EP-2015-xxx
April 4, 2018

Leading-order determination of the gluon polarisation using a novel method

The COMPASS Collaboration

Abstract

A re-evaluation of the gluon polarisation $\Delta g/g$ in the nucleon is presented, which is based on the measurement of the longitudinal double-spin asymmetry using semi-inclusive events with photon virtuality $Q^2 > 1 \text{ (GeV}/c)^2$. The data were obtained by the COMPASS experiment at CERN using a 160 GeV/c polarised muon beam scattering off a polarised ${}^6\text{LiD}$ target. The gluon polarisation is evaluated for three intervals of the nucleon momentum fraction carried by gluons, x_g , covering the range $0.04 < x_g < 0.28$. A novel method covering the full range in hadron transverse momentum p_T and a neural network approach are used. The values obtained at leading order in pQCD do not show any significant dependence on x_g . Averaged over the three intervals, the result is $\langle \Delta g/g \rangle = 0.113 \pm 0.038_{(\text{stat.})} \pm 0.036_{(\text{syst.})}$ at $\langle x_g \rangle \approx 0.10$ and a hard scale of $\mu^2 = \langle Q^2 \rangle = 3(\text{GeV}/c)^2$. The obtained result suggests that the gluon polarisation is positive in the measured x_g range.

(to be submitted to Phys. Lett. B)

The COMPASS Collaboration

C. Adolph⁹, M. Aghasyan²⁶, R. Akhunzyanov⁸, M.G. Alexeev²⁸, G.D. Alexeev⁸, A. Amoroso^{28,29}, V. Andrieux²², N.V. Anfimov⁸, V. Anosov⁸, W. Augustyniak³¹, A. Austregesilo¹⁷, C.D.R. Azevedo², B. Badełek³², F. Balestra^{28,29}, J. Barth⁵, R. Beck⁴, Y. Bedfer^{22,11}, J. Bernhard^{14,11}, K. Bicker^{17,11}, E. R. Bielert¹¹, R. Birsas²⁶, J. Bisplinghoff⁴, M. Bodlak¹⁹, M. Boer²², P. Bordalo^{13,a}, F. Bradamante^{25,26}, C. Braun⁹, A. Bressan^{25,26}, M. Büchele¹⁰, W.-C. Chang²³, M. Chiosso^{28,29}, I. Choi³⁰, S.-U. Chung^{17,b}, A. Cicuttin^{27,26}, M.L. Crespo^{27,26}, Q. Curiel²², S. Dalla Torre²⁶, S.S. Dasgupta⁷, S. Dasgupta^{25,26}, O.Yu. Denisov²⁹, L. Dhara⁷, S.V. Donskov²¹, N. Doshita³⁴, V. Duic²⁵, W. Dünneweber^c, M. Dziewiecki³³, A. Efremov⁸, P.D. Eversheim⁴, W. Eyrich⁹, M. Faessler^c, A. Ferrero²², M. Finger¹⁹, M. Finger jr.¹⁹, H. Fischer¹⁰, C. Franco¹³, N. du Fresne von Hohenesche¹⁴, J.M. Friedrich¹⁷, V. Frolov^{8,11}, E. Fuchey²², F. Gautheron³, O.P. Gavrichtchouk⁸, S. Gerassimov^{16,17}, F. Giordano³⁰, I. Gnesi^{28,29}, M. Gorzellik¹⁰, S. Grabmüller¹⁷, A. Grasso^{28,29}, M. Grosse Perdekamp³⁰, B. Grube¹⁷, T. Grussenmeyer¹⁰, A. Guskov⁸, F. Haas¹⁷, D. Hahne⁵, D. von Harrach¹⁴, R. Hashimoto³⁴, F.H. Heinsius¹⁰, R. Heitz³⁰, F. Herrmann¹⁰, F. Hinterberger⁴, N. Horikawa^{18,d}, N. d'Hose²², C.-Y. Hsieh²³, S. Huber¹⁷, S. Ishimoto^{34,e}, A. Ivanov^{28,29}, Yu. Ivanshin⁸, T. Iwata³⁴, R. Jahn⁴, V. Jary²⁰, R. Joosten⁴, P. Jörg¹⁰, E. Kabuß¹⁴, B. Ketzer⁴, G.V. Khaustov²¹, Yu.A. Khokhlov^{21,f,g}, Yu. Kisselev⁸, F. Klein⁵, K. Klimaszewski³¹, J.H. Koivuniemi³, V.N. Kolosov²¹, K. Kondo³⁴, K. Königsmann¹⁰, I. Konorov^{16,17}, V.F. Konstantinov²¹, A.M. Kotzinian^{28,29}, O.M. Kouznetsov⁸, M. Krämer¹⁷, P. Kremser¹⁰, F. Krinner¹⁷, Z.V. Kroumchtein⁸, Y. Kulinich³⁰, F. Kunne²², K. Kurek³¹, R.P. Kurjata³³, A.A. Lednev²¹, A. Lehmann⁹, M. Levillain²², S. Levorato²⁶, J. Lichtenstadt²⁴, R. Longo^{28,29}, A. Maggiora²⁹, A. Magnon²², N. Makins³⁰, N. Makke^{25,26}, G.K. Mallot¹¹, C. Marchand²², B. Marianski³¹, A. Martin^{25,26}, J. Marzec³³, J. Matoušek¹⁹, H. Matsuda³⁴, T. Matsuda¹⁵, G.V. Meshcheryakov⁸, W. Meyer³, T. Michigami³⁴, Yu.V. Mikhailov²¹, M. Mikhasenko⁴, Y. Miyachi³⁴, P. Montuenga³⁰, A. Nagaytsev⁸, F. Nerling¹⁴, D. Neyret²², V.I. Nikolaenko²¹, J. Nový^{20,11}, W.-D. Nowak¹⁰, G. Nukazuka³⁴, A.S. Nunes¹³, A.G. Olshevsky⁸, I. Orlov⁸, M. Ostrick¹⁴, D. Panzieri^{1,29}, B. Parsamyan^{28,29}, S. Paul¹⁷, J.-C. Peng³⁰, F. Pereira², M. Pešek¹⁹, D.V. Peshekhonov⁸, S. Platchkov²², J. Pochodzalla¹⁴, V.A. Polyakov²¹, J. Pretz^{5,h}, M. Quaresma¹³, C. Quintans¹³, S. Ramos^{13,a}, C. Regali¹⁰, G. Reicherz³, C. Riedl³⁰, M. Roskot¹⁹, N.S. Rossiyskaya⁸, D.I. Ryabchikov^{21,g}, A. Rybnikov⁸, A. Rychter³³, R. Salac²⁰, V.D. Samoilenko²¹, A. Sandacz³¹, C. Santos²⁶, S. Sarkar⁷, I.A. Savin⁸, T. Sawada²³, G. Sbrizzai^{25,26}, P. Schiavon^{25,26}, K. Schmidt^{10,j}, H. Schmieden⁵, K. Schönning^{11,i}, S. Schopferer¹⁰, E. Seder²², A. Selyunin⁸, O.Yu. Shevchenko^{8,*}, L. Silva¹³, L. Sinha⁷, S. Sirtl¹⁰, M. Slunecka⁸, J. Smolik⁸, F. Sozzi²⁶, A. Srnka⁶, M. Stolarski¹³, M. Sulc¹², H. Suzuki^{34,d}, A. Szabelski³¹, T. Szameitat^{10,j}, P. Sznajder³¹, S. Takekawa^{28,29}, M. Tasevsky⁸, S. Tessaro²⁶, F. Tessarotto²⁶, F. Thibaud²², F. Tosello²⁹, V. Tskhay¹⁶, S. Uhl¹⁷, J. Veloso², M. Virius²⁰, J. Vondra²⁰, T. Weisrock¹⁴, M. Wilfert¹⁴, J. ter Wolbeek^{10,j}, K. Zaremba³³, P. Zavada⁸, M. Zavertyaev¹⁶, E. Zemlyanichkina⁸, M. Ziembicki³³ and A. Zink⁹

¹ University of Eastern Piedmont, 15100 Alessandria, Italy

² University of Aveiro, Department of Physics, 3810-193 Aveiro, Portugal

³ Universität Bochum, Institut für Experimentalphysik, 44780 Bochum, Germany^{k1}

⁴ Universität Bonn, Helmholtz-Institut für Strahlen- und Kernphysik, 53115 Bonn, Germany^k

⁵ Universität Bonn, Physikalisches Institut, 53115 Bonn, Germany^k

⁶ Institute of Scientific Instruments, AS CR, 61264 Brno, Czech Republic^m

⁷ Matrivani Institute of Experimental Research & Education, Calcutta-700 030, Indiaⁿ

⁸ Joint Institute for Nuclear Research, 141980 Dubna, Moscow region, Russia^o

⁹ Universität Erlangen–Nürnberg, Physikalisches Institut, 91054 Erlangen, Germany^k

¹⁰ Universität Freiburg, Physikalisches Institut, 79104 Freiburg, Germany^{k1}

¹¹ CERN, 1211 Geneva 23, Switzerland

¹² Technical University in Liberec, 46117 Liberec, Czech Republic^m

- ¹³ LIP, 1000-149 Lisbon, Portugal^p
- ¹⁴ Universität Mainz, Institut für Kernphysik, 55099 Mainz, Germany^k
- ¹⁵ University of Miyazaki, Miyazaki 889-2192, Japan^q
- ¹⁶ Lebedev Physical Institute, 119991 Moscow, Russia
- ¹⁷ Technische Universität München, Physik Department, 85748 Garching, Germany^{kc}
- ¹⁸ Nagoya University, 464 Nagoya, Japan^q
- ¹⁹ Charles University in Prague, Faculty of Mathematics and Physics, 18000 Prague, Czech Republic^m
- ²⁰ Czech Technical University in Prague, 16636 Prague, Czech Republic^m
- ²¹ State Scientific Center Institute for High Energy Physics of National Research Center ‘Kurchatov Institute’, 142281 Protvino, Russia
- ²² CEA IRFU/SPhN Saclay, 91191 Gif-sur-Yvette, France^l
- ²³ Academia Sinica, Institute of Physics, Taipei, 11529 Taiwan
- ²⁴ Tel Aviv University, School of Physics and Astronomy, 69978 Tel Aviv, Israel^r
- ²⁵ University of Trieste, Department of Physics, 34127 Trieste, Italy
- ²⁶ Trieste Section of INFN, 34127 Trieste, Italy
- ²⁷ Abdus Salam ICTP, 34151 Trieste, Italy
- ²⁸ University of Turin, Department of Physics, 10125 Turin, Italy
- ²⁹ Torino Section of INFN, 10125 Turin, Italy
- ³⁰ University of Illinois at Urbana-Champaign, Department of Physics, Urbana, IL 61801-3080, U.S.A.
- ³¹ National Centre for Nuclear Research, 00-681 Warsaw, Poland^s
- ³² University of Warsaw, Faculty of Physics, 02-093 Warsaw, Poland^s
- ³³ Warsaw University of Technology, Institute of Radioelectronics, 00-665 Warsaw, Poland^s
- ³⁴ Yamagata University, Yamagata, 992-8510 Japan^q

* Deceased

^a Also at Instituto Superior Técnico, Universidade de Lisboa, Lisbon, Portugal

^b Also at Department of Physics, Pusan National University, Busan 609-735, Republic of Korea and at Physics Department, Brookhaven National Laboratory, Upton, NY 11973, U.S.A.

^c Supported by the DFG cluster of excellence ‘Origin and Structure of the Universe’ (www.universe-cluster.de)

^d Also at Chubu University, Kasugai, Aichi, 487-8501 Japan^q

^e Also at KEK, 1-1 Oho, Tsukuba, Ibaraki, 305-0801 Japan

^f Also at Moscow Institute of Physics and Technology, Moscow Region, 141700, Russia

^g Supported by Presidential grant NSh - 999.2014.2

^h Present address: RWTH Aachen University, III. Physikalisches Institut, 52056 Aachen, Germany

ⁱ Present address: Uppsala University, Box 516, SE-75120 Uppsala, Sweden

^j Supported by the DFG Research Training Group Programme 1102 “Physics at Hadron Accelerators”

^k Supported by the German Bundesministerium für Bildung und Forschung

^l Supported by EU FP7 (HadronPhysics3, Grant Agreement number 283286)

^m Supported by Czech Republic MEYS Grant LG13031

ⁿ Supported by SAIL (CSR), Govt. of India

^o Supported by CERN-RFBR Grant 12-02-91500

^p Supported by the Portuguese FCT - Fundação para a Ciência e Tecnologia, COMPETE and QREN, Grants CERN/FP 109323/2009, 116376/2010, 123600/2011 and CERN/FIS-NUC/0017/2015

^q Supported by the MEXT and the JSPS under the Grants No.18002006, No.20540299 and No.18540281; Daiko Foundation and Yamada Foundation

^r Supported by the Israel Academy of Sciences and Humanities

^s Supported by the Polish NCN Grant DEC-2011/01/M/ST2/02350

1 Introduction

The experimental observation by EMC [1] that quarks helicity constitutes only a small fraction of the nucleon spin was the starting point of new developments in spin physics, for a review see *e.g.* Ref. 2. In order to investigate the origin of the nucleon spin, it is essential to determine the nucleon spin fraction carried by gluon helicity, Δg . Information about this quantity can be obtained indirectly from scaling violations in the spin-dependent structure function g_1 (see Refs. 3–6 and references therein) or from a direct measurement of the gluon polarisation in polarised lepton-nucleon or proton-proton interactions (see Refs. 7–17). The value of Δg obtained from scaling violations is poorly constrained as its accuracy is limited by the kinematic range, in which the structure function g_1 is measured. On the other hand, the most recent fits performed in the context of perturbative Quantum Chromodynamics (pQCD) at next-to-leading order (NLO) in the strong coupling constant [18, 19], which include proton-proton data from RHIC, suggest that the gluon polarisation is positive in the measured range of the nucleon momentum fraction carried by gluons, $0.05 < x_g < 0.20$.

In deep inelastic scattering (DIS), the leading-order virtual-photon absorption process (LP) does not provide direct access to the gluon distribution since the virtual-photon does not couple to the gluon. Therefore, higher order processes have to be studied, *i.e.* QCD Compton scattering (QCDC) and Photon-Gluon Fusion (PGF), where only the latter is sensitive to the gluon helicity distribution. The diagrams for these two processes are shown in Fig. 1 together with that of the leading-order photon absorption process.

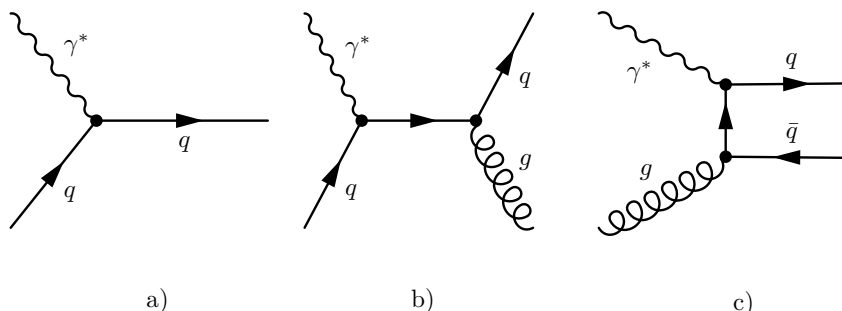


Fig. 1: Feynman diagrams for a) the leading-order process (LP), b) gluon radiation (QCDC), and c) photon-gluon fusion (PGF).

In the leading-order process, the hadron transverse momentum p_T with respect to the virtual-photon direction (in the frame where nucleon momentum is parallel to this direction) originates from the intrinsic transverse momentum k_T of the struck quark in the nucleon [20] and its fragmentation, which both lead to a small transverse component. On the contrary, the QCDC and PGF hard processes can provide hadrons with high transverse momentum. Therefore, tagging events with hadrons of large transverse momentum p_T enhances the contribution of higher-order processes. However, although in the high- p_T sample the PGF contribution is enriched, in order to determine $\Delta g/g$ the contributions from LP and QCDC have to be subtracted [21]. A different approach is used here, *i.e.* a simultaneous extraction of $\Delta g/g$ and the LP and QCDC asymmetries using data that cover the full range in p_T . This “all- p_T method” takes advantage of the different p_T dependences of the three processes to disentangle their contribution to the measured asymmetry. Furthermore, this approach reduces systematic uncertainties with respect to the one used previously [10]. In this Letter we re-analyse the semi-inclusive deep inelastic scattering (SIDIS) data from COMPASS [10], applying the new all- p_T method.

2 Experimental set-up and data sample

The COMPASS experiment is a fixed-target setup at the CERN SPS M2 beam line. For the present measurement, longitudinally polarised positive muons were scattered off a large polarised solid-state ${}^6\text{LiD}$ target. The data used in this analysis were collected during four years: 2002 to 2004 and 2006. A detailed description of the experiment can be found elsewhere [22]. A major upgrade of the COMPASS spectrometer was performed in 2005. For this analysis, the most relevant improvement was a new target magnet that extended the angular acceptance from ± 70 mrad to ± 180 mrad.

The average muon momentum was $160 \text{ GeV}/c$ and the average beam polarisation was $\langle P_b \rangle = -0.80 \pm 0.04$. The target material consisted of ${}^6\text{LiD}$ beads in a bath of ${}^3\text{He}$ - ${}^4\text{He}$ and was contained in two target cells in 2002–2004 and in three cells in 2006. The achieved target polarisation P_t was about ± 0.50 with a relative uncertainty of 5%. Neighbouring target cells were polarised in opposite directions. In order to cancel acceptance effects and to reduce systematic uncertainties, the direction of the polarisation was reversed three times per day in 2002–2004 and once per day in 2006. The fact that not all nucleons in the target material are polarisable is taken into account in the so-called effective dilution factor f . It is given by the ratio of the total cross section for muons on polarisable deuterons to the one on all nuclei taking into account their relative abundance in the target material. Its value includes a correction factor $\rho = \sigma_d^{1\gamma}/\sigma_d^{\text{tot}}$ [23] accounting for radiative events on unpolarised deuterons and a correction factor for the relative polarisation of deuterons bound in ${}^6\text{Li}$ compared to free deuterons. The dilution factor depends on the Bjorken scaling variable x_{Bj} and on the energy fraction y carried by the exchanged virtual-photon; the average value for this analysis is about 0.37 with a relative uncertainty of 5%.

The data used for this analysis is selected by requiring an event to have an interaction vertex located in the target fiducial volume. An incoming and a scattered muon must be associated to this vertex. Moreover, the extrapolation of the incoming muon track has to traverse fully all the target cells to expose them to the same beam flux. In order to select DIS events, the photon virtuality is required to be $Q^2 > 1 \text{ (GeV}/c)^2$. Events with $y < 0.1$ or $y > 0.9$ are rejected because the former are more sensitive to time instabilities of the spectrometer, while the latter are strongly affected by radiative effects. With these y limits, the squared invariant mass of the hadronic system, W^2 , is larger than $5 \text{ (GeV}/c)^2$. For the SIDIS analysis applied here, at least one charged hadron has to be associated to the vertex together with incoming and scattered muons. The hadron with the highest p_T has to fulfil the requirement $0.05 \text{ GeV}/c < p_T < 2.5 \text{ GeV}/c$. The lower limit excludes electrons from γ conversion; the upper limit is discussed in section 4. Events with exactly two oppositely charged hadrons and with the sum $z_1 + z_2$ of their energy fraction (relative to the virtual-photon energy) above 0.95 are removed to suppress diffractive processes (mainly ρ^0 production).

Compared to the previous analysis [10], there are two major differences in the selected data. Firstly, at least one hadron instead of two hadrons is required in the final state. Secondly, the p_T range for the hadron leading in p_T is extended to $0.05 \text{ GeV}/c < p_T < 2.5 \text{ GeV}/c$, while previously the lower limit was $0.7 \text{ GeV}/c$. After all cuts, about 116 million events remain for the present analysis.

3 Determination of $\Delta g/g$

The predicted number of events $N^{\text{pre}}(x_{\text{Bj}})$ can be calculated from the SIDIS cross sections of LP, QCDC, and PGF using the experimental acceptance a , the number of scattering centres in the target n , the integrated beam flux Φ , and the unpolarised cross section σ_0 as

$$N^{\text{pre}}(x_{\text{Bj}}) = an\Phi\sigma_0 \left(1 + \langle fP_bP_t a_{\text{LL}}^{\text{PGF}} R_{\text{PGF}} \frac{\Delta g}{g}(x_g) \rangle + \langle fP_bP_t a_{\text{LL}}^{\text{LP}} R_{\text{LP}} A_1^{\text{LP}}(x_{\text{Bj}}) \rangle + \langle fP_bP_t a_{\text{LL}}^{\text{QCDC}} R_{\text{QCDC}} A_1^{\text{QCDC}}(x_C) \rangle \right). \quad (1)$$

Here, the PGF part contains the gluon contribution to the nucleon spin, $\Delta g/g$. The two symbols A_1^{LP} and A_1^{QCDC} denote the same asymmetry¹; the distinction is only kept to emphasise the fact that in the new method there are two estimators of the same quantity. This fact will be used in some systematic studies presented in section 5. In Eq. (1), the predicted number of events depends only on the Bjorken scaling variable x_{Bj} , as other variables are integrated over the experimental kinematic domain. The label $i \in \{\text{LP}, \text{QCDC}, \text{PGF}\}$ refers to the processes presented in Fig. 1 and $x_{\text{LP}} \equiv x_{\text{Bj}}$, $x_{\text{QCDC}} \equiv x_{\text{C}}$, $x_{\text{PGF}} \equiv x_{\text{g}}$. For a given x_{Bj} , the corresponding nucleon momentum fractions carried by quarks in the QCDC process x_{C} and by the gluons x_{g} in the PGF process are in general larger and depend on the kinematics of the event. The relative contribution of the process i is denoted by R_i . The corresponding analysing power a_{LL}^i is given by the asymmetry of the partonic cross section [24]. It is proportional to the depolarisation factor D , which is the fraction of the muon polarisation transferred to the virtual-photon (for LP $a_{\text{LL}}^{\text{LP}} = D$). Equation (1) is valid at LO in QCD assuming spin-independent fragmentation. A possible spin dependence of the fragmentation process as discussed in Ref. 25 can be neglected in the COMPASS kinematic region. Equation (1) can be written in a more concise form as

$$N^{\text{pre}}(x_{\text{Bj}}) = \alpha \left(1 + \sum_i \langle \beta_i A^i(x_i) \rangle \right). \quad (2)$$

Here, $\alpha = an\Phi\sigma_0$, $\beta_i = fP_b P_i a_{\text{LL}}^i R_i$ and $\langle \beta_i A^i(x_i) \rangle$ denotes the average of $\beta_i A^i(x_i)$ over the experimental kinematic domain. For simplicity the x_i dependence of β_i is omitted.

The data were taken simultaneously for the upstream (u) and downstream (d) target cells, in which the material was polarised longitudinally in opposite directions. For 2006 the label u refers to the two outer cells and d to the central cell. The directions of the polarisation are periodically reversed, yielding the event counts (N_u, N_d) before and ($N_{u'}, N_{d'}$) after a reversal. For a stable apparatus it is expected that $\alpha_u/\alpha_d = \alpha_{u'}/\alpha_{d'}$. The data sample was divided into 40 periods, over which the apparatus was indeed found to be stable. The analysis is performed independently in each of the periods. The final result is obtained as the weighted average of the 40 results.

The evaluation of $\Delta g/g$ using the set of equations obtained from Eq. (1) for the various target cells and polarisations is possible only if the contributions from background processes (LP, QCDC) can be computed and subtracted. The process fractions R_i , the momentum fractions x_{C} , x_{g} , and the analysing powers $a_{\text{LL}}^{\text{QCDC}}$, $a_{\text{LL}}^{\text{PGF}}$ are determined using Monte Carlo (MC) simulations. In a previous paper [10], the asymmetry A_1^{LP} was evaluated from the inclusive lepton–nucleon asymmetry $A_{\text{LL}}^{\text{incl}}$. In this analysis, A_1^{LP} is extracted simultaneously with $\Delta g/g$ from the same data.

The method applied here was introduced in Ref. 26 and already used for a gluon polarisation determination from open charm events [11]. In order to extract simultaneously the signal $\Delta g/g$ and the background asymmetries A_1^{LP} and A_1^{QCDC} , the event yields are considered separately for the three processes i . Moreover, since $\Delta g/g$, A_1^{LP} , and A_1^{QCDC} are known to be x_i dependent, the analysis is performed in bins of the corresponding x_i variable indexed by m . For each configuration $k = u, d, u', d'$ we calculate weighted ‘predicted’ and ‘observed’ event yields, $\mathcal{N}_{i,m,k}^{\text{pre}}$ and $\mathcal{N}_{i,m,k}^{\text{obs}}$, respectively. Using the weight $w = fP_b a_{\text{LL}} R$, the observed weighted yield of events for the process i in the m^{th} bin of x_i is given by summing the corresponding weights $w_{i,n}$:

$$\mathcal{N}_{i,m,k}^{\text{obs}} = \sum_{n=1}^{N_k} \epsilon_{m,i} w_{i,n} = \sum_{n=1}^{N_k} \epsilon_{m,i} f_n P_{b,n} a_{\text{LL},n}^i R_{i,n}. \quad (3)$$

The sum runs over the number of events N_k observed for configuration k , and $\epsilon_{m,i}$ is equal to 1 if the given

¹ They are also equivalent to $A_1^{\text{LO}}(x)$ from Ref. 10, see Eq. (1) *ibid*.

event x_i belongs to its m^{th} bin, and zero otherwise. The target polarisation is not included in the weight because its value changes with time. Since one knows only the probabilities R_i that the event originated from a particular partonic process, each event contributes to all three event yields $\mathcal{N}_{\text{PGF}_m,k}^{\text{obs}}$, $\mathcal{N}_{\text{QCDC}_{m'},k}^{\text{obs}}$, and $\mathcal{N}_{\text{LP}_{m'},k}^{\text{obs}}$. The correlation between these events yields is taken into account by the covariance matrix $\text{COV}_{i_m j_{m'},k} = \sum_{n=1}^{N_k} \epsilon_{m,i} \epsilon_{m',j} w_{i,n} w_{j,n}$.

The predicted weighted yields of events of each type, $\mathcal{N}_{i_m,k}^{\text{pre}}$, is approximated by

$$\mathcal{N}_{i_m,k}^{\text{pre}} \approx \alpha_{k,w_{i_m}} \left(1 + \sum_j \sum_{m'} \langle \beta_{j_{m'}} \rangle_{w_{i_m}} \langle A^j(x_j) \rangle_{m'} \right), \quad (4)$$

where $\alpha_{k,w_{i_m}}$ is the weighted value of α_k ($\alpha_{u,w_{i_m}} / \alpha_{d,w_{i_m}} = \alpha_{u',w_{i_m}} / \alpha_{d',w_{i_m}}$) and

$$\langle \beta_{j_{m'}} \rangle_{w_{i_m}} \approx \frac{\sum_{n=1}^{N_k} \epsilon_{m,i} \epsilon_{m',j} \beta_{j,n} w_{i,n}}{\sum_{n=1}^{N_k} \epsilon_{m,i} w_{i,n}}. \quad (5)$$

Here, the additional assumption $\langle \beta_j A^j(x_j) \rangle \simeq \langle \beta_j \rangle \langle A^j(x_j) \rangle$ was used. Knowing the number of observed and predicted events as well as the covariance matrix, the standard definition of χ^2 is used, $\chi^2 = (\mathcal{N}^{\text{obs}} - \mathcal{N}^{\text{pre}})^T \text{COV}^{-1} (\mathcal{N}^{\text{obs}} - \mathcal{N}^{\text{pre}})$, where \mathcal{N}^{obs} and \mathcal{N}^{pre} are vectors with the components $\mathcal{N}_{i_m,k}^{\text{obs}}$ and $\mathcal{N}_{i_m,k}^{\text{pre}}$, respectively. The values of $\Delta g/g$, A_1^{LP} and A_1^{QCDC} are obtained from the minimisation of χ^2 by the MINUIT programme [27]. The HESSE method from the same package is used to calculate the uncertainties. In the present analysis we use 12 bins in x_{Bj} , 6 in x_{C} and in 1 or 3 bins in x_{g} . In the COMPASS kinematic region $x_{\text{C}} \gtrsim 0.06$ so that the same binning can be used for x_{C} as for the six highest bins in x_{Bj} . In order to further constrain $\Delta g/g$, one can eliminate several parameters from the fit by using the relation $A_1^{\text{LP}}(x) = A_1^{\text{QCDC}}(x)$.

The sample of low- p_{T} events is almost entirely dominated by the LP process. It thus provides to the applied χ^2 minimisation enough lever-arm for a separation between the LP and PGF processes, allowing the simultaneous extraction of their asymmetries. As a result, a significant reduction of both statistical and systematic uncertainties is achieved when comparing to Ref. 10.

The presented method of the extraction of $\Delta g/g$ is model dependent. Model-independent quantities that can be used in future NLO analyses of $\Delta g/g$, are longitudinal double-spin asymmetries with a hadron in the final state, A_{LL}^{h} . They were extracted in bins of x_{Bj} and p_{T} of the hadron leading in p_{T} and are available in [28]. Observe, that these asymmetries are not used directly in the all- p_{T} method presented in this Letter.

4 Monte Carlo Simulation and Neural Network Training

The LEPTO event generator [29] (version 6.5) is used to generate the MC using the unpolarised cross sections of the three processes involved. The generated events are processed by the detector simulation programme COMGEANT (based on GEANT3) and reconstructed in the same way as real events by the reconstruction programme CORAL. The same data selection is then applied to real and Monte Carlo events. In Ref.30 it was found that simulations with the two hadron-shower models available in GEANT3 (GHEISHA and FLUKA) give inconsistent results in the high- p_{T} region. Therefore, it was decided to skip in the analysis those events, for which the hadron leading in p_{T} has $p_{\text{T}} > 2.5 \text{ GeV}/c$.

The best description of the data in terms of data-to-MC ratios for various variables is obtained when using LEPTO with the parton shower mechanism switched on, the fragmentation function tuning as described in Ref.10, and the PDF set of MSTW08LO_{3fl} from Ref. 31 together with the F_L function option from LEPTO. A correction for radiative effects as described in Ref. 23 is applied. In Fig. 2 data and MC are

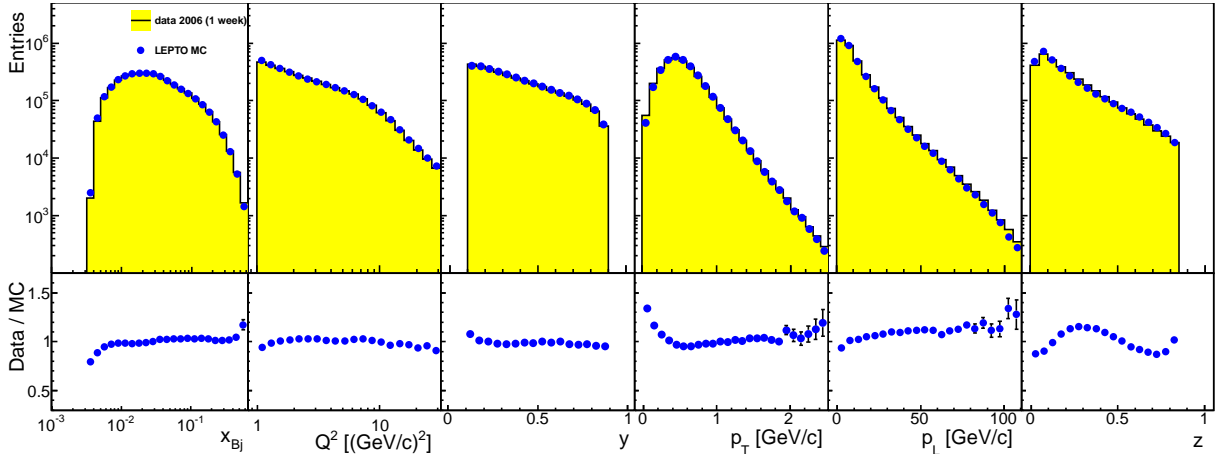


Fig. 2: Comparison of kinematic distributions from data and MC simulations (top panels) and their ratio (bottom panels) for the lepton variables: x_{Bj} , Q^2 , y and for p_T , p_L and z of the hadron leading in p_T , normalised to the number of events.

compared for the lepton variables, x_{Bj} , Q^2 , y and for p_T , p_L and z of the hadron leading in p_T . The Monte Carlo simulation describes the data reasonably well over the full phase space. The largest discrepancy is observed for low p_T values, where the LP is dominant. Therefore, this region has limited impact on the extracted $\Delta g/g$ value. The best description of the data in terms of data-to-MC ratios was the reason to select the presented MC sample for the extraction of the final $\Delta g/g$ value.

For a given set of input parameters, a neural network (NN) is trained to output the corresponding expectation value for fractions R_i , x_i and analysing powers a_{LL}^i . The input parameter space is defined by x_{Bj} , Q^2 and by p_L , p_T of the hadron leading in p_T . The same type of neural network from Ref. 32 is used as in Ref. 10. In the case that a clear distinction between the ‘true’ MC value and its NN parametrisation is needed, for the latter one the superscript ‘NN’ will be added to the symbol denoting this variable, *e.g.* x_g^{NN} . An example of the quality of the NN parametrisation is given in the top panels of Fig. 3. It shows ‘true’ probabilities for LP, QCDC and PGF events as a function of p_T and the NN probabilities obtained for the same MC data. While the LP probability falls with increasing p_T , QCDC and PGF rise with comparable strength. Another NN quality test is presented in the bottom panels of Fig. 3, where MC samples are selected in bins of the R_i values returned by the NN, which corresponds to the probability that the given event is of type i . Using the true MC information, it is possible to verify the generated fraction of processes i in the selected samples. A very good correlation is visible between NN output and the true MC composition.

5 Systematic Studies

With respect to the analysis method used in Ref. 10, two contributions to the systematic uncertainty are eliminated, *i.e.* the one related to the x_C approximation² and the one related to the parametrisation of $A_{1,d}^{\text{incl}}$. The other major contributions to the systematic uncertainty are re-evaluated in the current analysis. These are the limit on experimental false asymmetries, δ_{false} , the uncertainty related to the usage of MC in the analysis, δ_{MC} , the impact of using a NN on the results, δ_{NN} , and the uncertainty that is obtained by combining those of beam and target polarisations and of the dilution factor, which is denoted as $\delta_{P_b P_t}$. All these contributions to the systematic uncertainty are given in Table 1 for the $\Delta g/g$ results obtained in the full x_g range and for those obtained in three bins of x_g^{NN} . The systematic uncertainty of the $\Delta g/g$ result, δ_{sys} , is calculated as quadratic sum of the contributions δ_{false} , δ_{MC} , δ_{NN} , and $\delta_{P_b P_t}$.

The false asymmetries are related to the stability of the spectrometer. The contribution of $\delta_{\text{false}} = 0.029$

²*i.e.* $x_C = x_{C'}$ in Eq. (3) of [10].

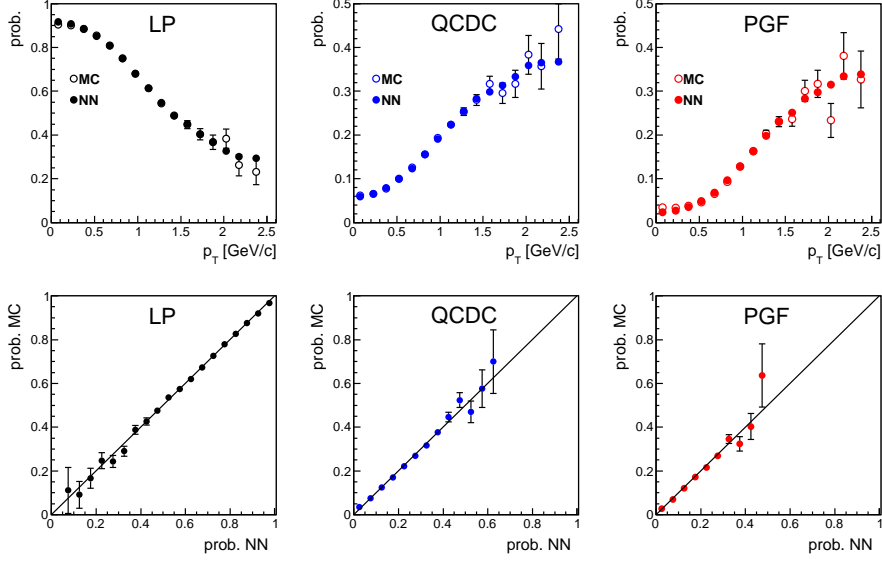


Fig. 3: Top panels: Values of R_{LP} , R_{QCDC} , R_{PGF} obtained from MC and NN as a function of p_T . Bottom panels: MC probabilities in bins of NN probabilities.

Table 1: Summary of contributions to the systematic uncertainty.

syst. unc.	full x_g range	$x_g^{NN} < 0.10$	$0.10 < x_g^{NN} < 0.15$	$x_g^{NN} > 0.15$
δ_{false}	0.029	0.039	0.022	0.014
δ_{MC}	0.017	0.017	0.041	0.044
δ_{NN}	0.007	0.007	0.007	0.018
$\delta_{P_b P_f}$	0.010	0.008	0.013	0.013
$\delta_{\text{sys.}}$	0.036	0.044	0.049	0.051

is somewhat larger than that obtained in the previous analysis [10], where it was additionally assumed that false asymmetries are independent of p_T ³.

Although the present analysis depends on the MC model used, the uncertainty δ_{MC} is found to be small. It is evaluated by exploring the parameter space of the model using eight different MC simulations. These eight simulations differ by the tuning of the fragmentation functions (COMPASS High- p_T , [10] or LEPTO default), and by using or not using of the parton shower (PS) mechanism, which also modifies the cut-off schemes used to prevent divergences in the LEPTO cross-section calculation [29]. Also, different PDF sets are used (MSTW08L or CTEQ5L [33]), the longitudinal structure function F_L from LEPTO is used or not used and alternatively FLUKA or GEISHA is used for the simulation of secondary interactions. Two observations are made when inspecting Fig. 4. The first one is that for the eight different MC simulations the resulting values of $\Delta g/g$ are very similar; the root mean square (RMS) of the eight values, which is taken to represent δ_{MC} , amounts to only 0.017. The second observation is that the eight statistical uncertainties vary by up to a factor of two.

The explanation for the second observation is that in a good approximation the statistical uncertainty of $\Delta g/g$ is proportional to $1/R_{\text{PGF}}$. As in the eight different MC simulation the values of R_{PGF} can vary by up to a factor two, large fluctuations of statistical uncertainties of $\Delta g/g$ are observed in Fig. 4. The observation of a small RMS value can be understood by the following consideration. Assuming that

³This assumption, when used in the current analysis, would lead to a much lower value of δ_{false} than previously. This is due to the simultaneous extraction of $\Delta g/g$ and A_1^{LP} , which are both affected by the same spectrometer instabilities, thereby eliminating relative contributions to δ_{false} .

Eq. (1) in Ref. 10 is re-written for the one-hadron case, and that the left-hand side of the equation is cancelled by the second term on the right-hand side, $\Delta g/g$ is approximated as

$$\Delta g/g \approx -\frac{a_{LL}^{\text{QCDC}} R_{\text{QCDC}}}{a_{LL}^{\text{PGF}} R_{\text{PGF}}} A_1^{\text{LP}}(\langle x_C \rangle \approx 0.14). \quad (6)$$

The value of A_1^{LP} at $\langle x_C \rangle = 0.14$ is ≈ 0.087 , while the value of $(a_{LL}^{\text{QCDC}} R_{\text{QCDC}})/(a_{LL}^{\text{PGF}} R_{\text{PGF}})$ is ≈ 1.5 , giving $\Delta g/g \approx 0.13$. This value is not very different from the result of the full analysis presented in section 6, which justifies the usage of Eq. (6) for the explanation of the small RMS. The values of a_{LL}^{PGF} and a_{LL}^{QCDC} in Eq. (6) are quite stable with respect to the MC simulation used. As a_{LL}^{PGF} depends mostly on Q^2 and y , which as inclusive variables are not affected by switching parton showers on or off nor by different fragmentation tunes, it is very similar in all eight MC simulations. A similar consideration is valid for a_{LL}^{QCDC} , which depends mostly on y . The ratio $R_{\text{QCDC}}/R_{\text{PGF}}$ is known more precisely than *e.g.* the ratio $R_{\text{LP}}/R_{\text{PGF}}$ or R_{PGF} itself. One reason here is that both QCDC and PGF are treated in NLO, so that the strong coupling constant cancels in the cross section ratio. In addition, the hadron p_T in both processes is dominated by the partonic cross section calculable in LO pQCD and not by the fragmentation process, for which the parameters were tuned.

The usage of NN method leads to a systematic uncertainty $\delta_{\text{NN}} = 0.007$. The systematic uncertainty δ_{P_f} , which is proportional to the extracted value of $\Delta g/g$ in the all- p_T method, is evaluated to be 0.010. The systematic uncertainties due to radiative corrections, due to the resolved-photon contribution, and due to remaining contributions from diffractive processes are estimated to be small and can hence be safely neglected.

In the present analysis method, A_1^{LP} and A_1^{QCDC} are two estimators of the same quantity. This fact allows to perform additional consistency checks of the MC model used in the analysis, which were not possible in the analysis method used in Ref. 10. The validity of the assumption $A_1^{\text{LP}}(x) = A_1^{\text{QCDC}}(x)$ can be verified by performing a standard χ^2 test. A possible failure of a χ^2 test may indicate the use of incorrect R_i and/or a_{LL}^i values in the analysis. This could happen if the MC tuning used in the analysis is wrong, or *e.g.* higher order corrections are substantial. This compatibility check was performed for all eight MC samples, giving a χ^2 value between 3.9 and 13.1 for 6 degrees of freedom. For the MC simulation used to obtain the quoted $\Delta g/g$ value, $\chi^2 = 8.1$ was found, which means that values of A_1^{QCDC} and A_1^{LP} are compatible. Furthermore, one can also directly change the values of *e.g.* $a_{LL}^{\text{QCDC}} R_{\text{QCDC}}$ obtained from NN, and by checking the compatibility of the two A_1 values verify the consistency of data and MC model. In the simplest test, we have added a multiplicative factor η_{QCDC} to the MC value of $a_{LL}^{\text{QCDC}} R_{\text{QCDC}}$ and calculated the χ^2 value of the compatibility test as a function of η_{QCDC} . As seen in the right panel of Fig. 4, the minimum value of χ^2 is obtained for $\eta_{\text{QCDC}} \approx 1$, which supports the validity of the MC model.

The present analysis method assumes that A_1^{LP} and $\Delta g/g$ are independent of p_T . We have verified that using different minimum p_T cuts between 0.05 GeV/ c and 1 GeV/ c for data selection the extracted values of A_1^{LP} and $\Delta g/g$ are compatible within statistical uncertainties with the final results, when taking into account correlations of the data samples.

6 Results

The re-evaluation of the gluon polarisation in the nucleon yields

$$\langle \Delta g/g \rangle = 0.113 \pm 0.038_{(\text{stat.})} \pm 0.036_{(\text{sys.})}, \quad (7)$$

which is obtained at average hard scale $\mu^2 = \langle Q^2 \rangle = 3 \text{ (GeV}/c)^2$. In the analysis, a correction is applied to account for the probability that the deuteron is in a D-wave state [34]. In the kinematic domain of the analysis, the average value of x_g , weighted by $a_{LL}^{\text{PGF}} w_{\text{PGF}}$, is $\langle x_g \rangle \approx 0.10$. In the case that $\Delta g/g$

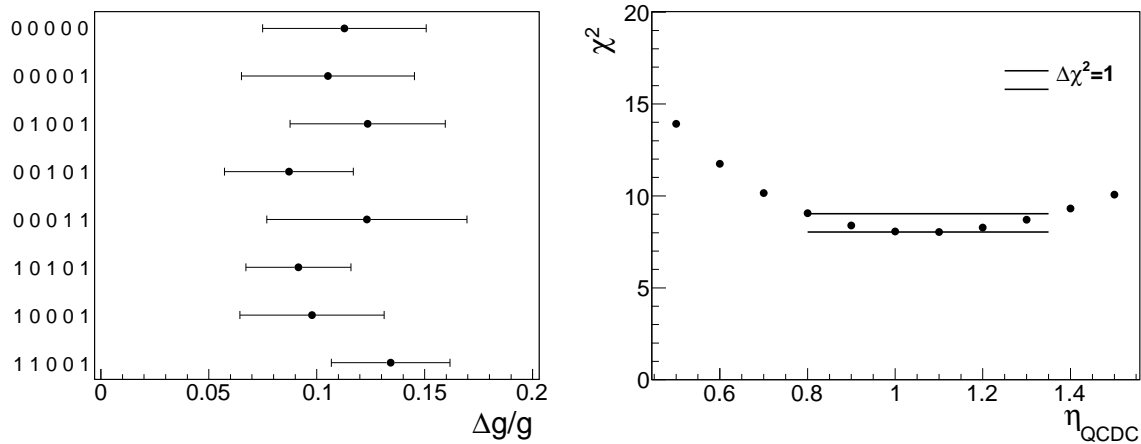


Fig. 4: Left panel: Extracted values of $\Delta g/g$ and their statistical uncertainties for eight different MC simulations. A digit ‘1’ at a certain position in the 5-digit code shown on the ordinate means that the corresponding simulation parameter was used differently as compared to the code 00000 simulation that was used for the extraction of the final $\Delta g/g$ results. The meaning of the digits is as follows (from left to right): 1st choice of the fragmentation functions tuning; 2nd usage of PS mechanism (here 0 means ON); 3rd choice of PDF; 4th usage of F_L function from LEPTO (here 0 means ON); and 5th choice of a program to simulate secondary interactions. Right panel: The results of the χ^2 scan of η_{QDC} , see text for details.

can be approximated by a linear function in the measured region of x_g , the obtained results of $\langle \Delta g/g \rangle$ corresponds to a value of $\Delta g/g$ at this weighted average value of x_g . The obtained value of $\Delta g/g$ is positive in the measured x_g range and almost $3\sigma_{\text{stat}}$ from zero. A similar conclusion is reached in the NLO pQCD fits [18, 19], which include recent RHIC data. The present result agrees well with the previous one [10] that was obtained from the same data ($\Delta g/g = 0.125 \pm 0.060 \pm 0.065$). This comparison shows that the re-analysis using the new all- p_T method leads to a reduction of the statistical and systematic uncertainty by a factor of 1.6 and 1.8, respectively.

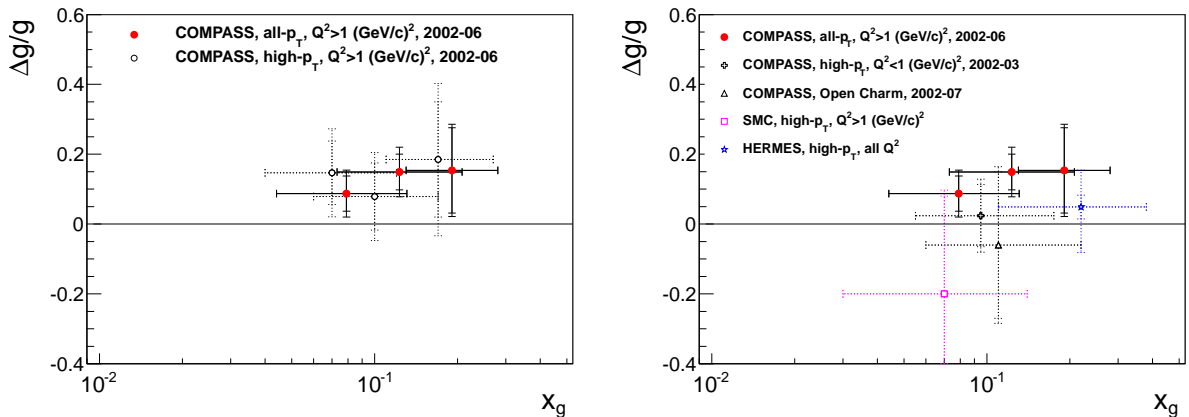
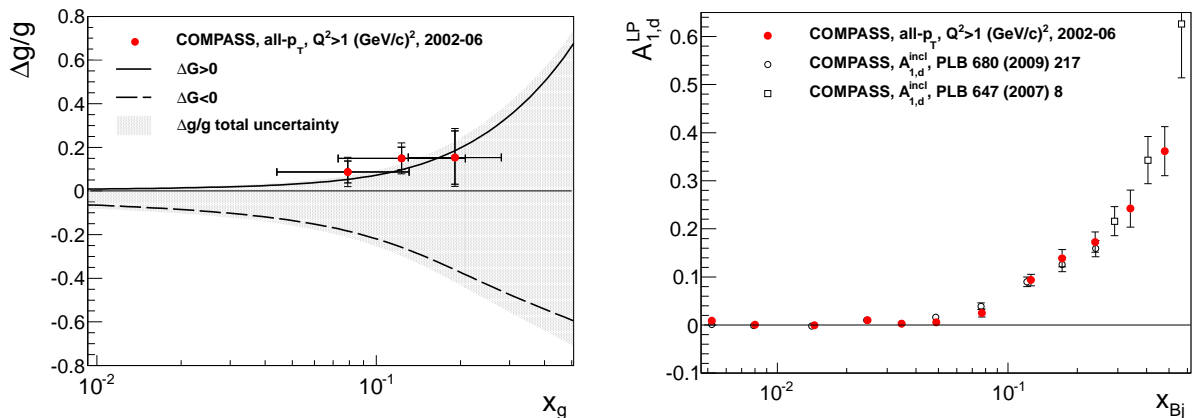
The gluon polarisation is also determined in three bins of x_g^{NN} , which correspond to three ranges in x_g . These ranges are partially overlapping due to an about 60% correlation between x_g and x_g^{NN} , which arises during the NN training. The result on $\Delta g/g$ in three bins of x_g^{NN} are presented in Table 2. Within experimental uncertainties, the values do not show any significant dependence on x_g . Note that the events in the three bins of x_g^{NN} are statistically independent. In principle, for each x_g^{NN} bin one could extract simultaneously $\Delta g/g$ and A_1^{LP} in 12 x_{Bj} bins, resulting in 36 A_1^{LP} and three $\Delta g/g$ values. However, in order to minimise statistical uncertainties of the obtained $\Delta g/g$ values, for a given x_{Bj} bin only one value of A_1^{LP} is extracted instead of three. As a result of such a procedure, a correlation between the three $\Delta g/g$ results may arise from the fit. Indeed, a 30% correlation is found between $\Delta g/g$ results obtained in the first and second x_g^{NN} bins. The correlations of the results between the first or second and the third x_g^{NN} bin are found to be consistent with zero.

A comparison of the published [10] and present results is shown in the left panel of Fig. 5. In addition to a clear reduction of the statistical uncertainties, a small shift in the average value of x_g is observed, which originates from using slightly different data selection criteria in the all- p_T analysis and also from differences between the two methods. In the right panel of Fig. 5, the new results are compared with the world results on $\Delta g/g$ extracted in LO analyses [7–9, 11], and good agreement is observed. The new COMPASS results have the smallest combined statistical and systematic uncertainty.

The left panel of Fig. 6 shows the present results, which are obtained at LO, in comparison to the most

Table 2: The values for $\langle \Delta g/g \rangle$ in three x_g^{NN} bins, and for the full x_g range.

x_g^{NN} bin	$\langle x_g \rangle$	x_g range (RMS)	$\langle \Delta g/g \rangle$
0–0.10	0.08	0.04 – 0.13	$0.087 \pm 0.050 \pm 0.044$
0.10–0.15	0.12	0.07 – 0.21	$0.149 \pm 0.051 \pm 0.049$
0.15–1	0.19	0.13 – 0.28	$0.154 \pm 0.122 \pm 0.051$
0–1	0.10	0.05 – 0.20	$0.113 \pm 0.038 \pm 0.036$

**Fig. 5:** The new results for $\Delta g/g$ in three x_g bins compared to results of Ref. 10 (left panel) and world data on $\Delta g/g$ extracted in LO [7–9, 11] (right panel). The inner error bars describe the statistical uncertainties, and the outer ones describe the statistical and systematic uncertainties combined in quadrature. The horizontal error bars describe x_g range (RMS).**Fig. 6:** Left panel: Comparison of the new LO results with the newest COMPASS NLO QCD fit [35]. Otherwise as in Fig. 5. Right panel: Extracted values of $A_{1,d}^{\text{LP}}(x_{Bj})$ and $A_{1,d}^{\text{incl}}$ from [5, 36]. Here, only statistical uncertainties are shown.

recent COMPASS NLO $\Delta g/g$ parametrisation [35]. The present results support solutions with positive ΔG value for the fit. Note that this comparison does not account for the difference between LO and NLO.

For completeness, in the right panel of Fig. 6 the extracted values of $A_{1,d}^{\text{LP}}(x_{Bj})$ are shown as full points. They are consistent with zero at low x_{Bj} and rise at higher x_{Bj} . The LP measured in this analysis is the major contributor to the inclusive asymmetry $A_{1,d}^{\text{incl}}$, and the values of $A_{1,d}^{\text{LP}}$ and $A_{1,d}^{\text{incl}}$ shows very similar trends, as expected. The values of $A_{1,d}^{\text{incl}}$ for $x_{Bj} < 0.3$ are from Ref. 36 while those for $x_{Bj} > 0.3$ are from Ref. 5.

7 Conclusions

The re-evaluation of the gluon polarisation in the nucleon yields at LO in pQCD $\langle \Delta g/g \rangle = 0.113 \pm 0.038_{(\text{stat.})} \pm 0.036_{(\text{syst.})}$ for a weighted average of $\langle x_g \rangle \approx 0.10$ and an average hard scale of $3 \text{ (GeV}/c)^2$. This result is compatible with and supersedes our previous result [10] obtained from the same $Q^2 > 1 \text{ (GeV}/c)^2$ data. It favours a positive gluon polarisation in the measured x_g range. The new ‘all- p_T method’ employed in the present analysis leads to a reduction of both the statistical and systematic uncertainties on the gluon polarisation. This is due to the cancellation of some uncertainties in the simultaneous determination of $\Delta g/g$ and $A_{1,d}^{\text{LP}}$.

Acknowledgements

We gratefully acknowledge the support of the CERN management and staff and the skill and effort of the technicians of our collaborating institutes. This work was made possible thanks to the financial support of our funding agencies.

References

- [1] EMC Collaboration, J. Ashman *et al.*, Phys. Lett. B **206** (1988) 364; Nucl. Phys. B **328** (1989) 1.
- [2] C. A. Aidala, S. D. Bass, D. Hasch and G. K. Mallot, Rev. Mod. Phys. **85** (2013) 655.
- [3] SMC Collaboration, B. Adeva *et al.*, Phys. Rev D **58** (1998) 112002.
- [4] E155 Collaboration, P. L. Anthony *et al.*, Phys. Lett. B **493** (2000) 19.
- [5] COMPASS Collaboration, V. Yu. Alexakhin *et al.*, Phys. Lett. B **647** (2007) 8.
- [6] HERMES Collaboration, A. Airapetian *et al.*, Phys. Rev. D **75** (2007) 012007.
- [7] SMC Collaboration, B. Adeva *et al.*, Phys. Rev. D **70** (2004) 012002.
- [8] COMPASS Collaboration, E. S. Ageev *et al.*, Phys. Lett. B **633** (2006) 25.
- [9] HERMES Collaboration, A. Airapetian *et al.*, Journal of High Energy Physics **1008** (2010) 130.
- [10] COMPASS Collaboration, C. Adolph *et al.*, Phys. Lett. B **718** (2013) 922.
- [11] COMPASS Collaboration, C. Adolph *et al.*, Phys. Rev. D **87** (2013) 052018.
- [12] STAR Collaboration, L. Adamczyk *et al.*, Phys. Rev. D **89** (2014) 012001.
- [13] PHENIX Collaboration, A. Adare *et al.*, Phys. Rev. D **90** (2014) 012007.
- [14] PHENIX Collaboration, A. Adare *et al.*, Phys. Rev. D **84** (2011) 012006.
- [15] STAR Collaboration, L. Adamczyk *et al.*, Phys. Rev. Lett. **115** (2015) 092002.
- [16] PHENIX Collaboration, A. Adare *et al.*, Phys. Rev. Lett. **106** (2011) 062001.
- [17] STAR Collaboration, L. Adamczyk *et al.*, Phys. Rev. Lett. **113** (2014) 072301.
- [18] D. de Florian, R. Sassot, M. Stratmann and W. Vogelsang, Phys. Rev. Lett. **113** (2014) 012001.
- [19] E. R. Nocera, R. D. Ball, S. Forte, G. Ridolfi and J. Rojo, Nucl. Phys. B **887** (2014) 276.
- [20] P. Renton and W. S. C. Williams, Ann. Rev. Nucl. Sci. **31** (1981) 193.
- [21] A. Bravar, D. von Harrach and A. Kotzinian, Phys. Lett. B **421** (1998) 349.
- [22] COMPASS Collaboration, P. Abbon *et al.*, Nucl. Instrum. and Meth. A **577** (2007) 455.
- [23] A. A. Akhundov, D. Yu. Bardin, L. Kalinovskaya and T. Riemann, Fortschr. Phys. **44** (1996) 373.
- [24] A. Bravar, K. Kurek and R. Windmolders, Comput. Phys. Commun. **105** (1997) 42.
- [25] A. Kotzinian, Eur. Phys. J. C **44** (2005) 211.
- [26] J. Pretz and J.-M. Le Goff, Nucl. Instrum. Meth. A **602** (2009) 594.
- [27] F. James and M. Roos, Comput. Phys. Commun. **10** (1975) 343.
- [28] The Durham HepData Project, <http://hepdata.cedar.ac.uk/>.

- [29] G. Ingelman, A. Edin and J. Rathsman, *Comput. Phys. Commun.* **101** (1997) 108.
- [30] COMPASS Collaboration, C. Adolph *et al.*, *Phys. Rev. D* **88** (2013) 091101.
- [31] A. D. Martin, W. J. Stirling, R. S. Thorne and G. Watt, *Eur. Phys. J. C* **64** (2009) 653.
- [32] R. Sulej, *NetMaker*, <http://www.ire.pw.edu.pl/~rsulej/NetMaker/>.
- [33] CTEQ Collaboration, H. L. Lai *et al.*, *Eur. Phys. J. C* **12** (2000) 375.
- [34] R. Machleidt *et al.*, *Phys. Rep.* **149** (1987) 1.
- [35] COMPASS Collaboration, C. Adolph *et al.*, *subm. to Phys. Lett. B*, hep-ex/1503.08935 .
- [36] COMPASS Collaboration, M. Alekseev *et al.*, *Phys. Lett. B* **680** (2009) 217.
- [37] COMPASS Collaboration, E. S. Ageev *et al.*, *Phys. Lett. B* **612** (2005) 154.